IEEE Access
Multidisciplinary ⋮ Rapid Review ⋮ Open Access Journal

Received 16 August 2023, accepted 7 September 2023, date of publication 13 September 2023,
date of current version 19 September 2023.

Digital Object Identifier 10.1109/ACCESS.2023.3314758

RESEARCH ARTICLE

Tangential Electromagnetic Force Array on the Vibration and Noise of Electric Axle for New Energy Vehicle

CHAO HUANG[1], LU XIONG[1], YU GONG[2], MINGYUAN JIANG[3], AND SHUANGXIA NIU[3], (Senior Member, IEEE)

[1]School of Automotive Studies, Tongji University, Shanghai 201804, China
[2]Schaeffler Trading (Shanghai) Company Ltd., Shanghai 201804, China
[3]Department of Electrical and Electronic Engineering, The Hong Kong Polytechnic University, Hong Kong, China

Corresponding author: Mingyuan Jiang (ming-yuan.jiang@connect.polyu.hk)

ABSTRACT It is generally accepted that the vibration and noise of electrical motors mainly depend on radial electromagnetic forces. However, the relationship between electromagnetic forces and system modes becomes special when integrating the electrical motor into a coaxial electric axle (eAxle). This paper proposes a phase-based tangential electromagnetic force array analysis method to explain and optimize the noise spikes in a coaxial eAxle which is driven by a permanent magnet synchronous motor (PMSM) with a step-skewed rotor. Its electromagnetic force on each stator node is decomposed into radial and tangential forces as inputs for structural finite element simulation. Based on their contributions to the noise, the torsional vibration and noise of the eAxle are correlated with the tangential electromagnetic force array. Thus, the coupling effect of excitation and response is illustrated, and the electromagnetic force array could be optimized more targeted.

INDEX TERMS PMSM, tangential electromagnetic force, torsional mode.

I. INTRODUCTION

Electric vehicles have developed rapidly in recent years due to their green, quiet, and efficient nature. As the key component of the powertrain, the drive motor is crucial to the performance of the vehicle. Compared to electrically excited motors, permanent magnet synchronous motors (PMSM) are widely used in powertrains such as electric axles (eAxle) because they have no excitation losses and are more efficient in the low to medium speed ranges. On the other hand, the peak torque and power density of electric motors are increasing to reduce the size and weight of the system. The high energy density poses a serious challenge to the vibration and noise in new energy vehicles.

The electromagnetic noise of electric motors originates from the electromagnetic force generated by the stator and rotor magnetic fields. Since the 1970s, the magnetic flux density in the airgap of induction motors has been analyzed in detail [1]. In the 1990s, with the application of permanent magnet motors, the electromagnetic vibration and noise of PMSMs were analyzed [2], [3], [4]. In recent years, with the development of numerical simulation techniques and test equipment, the vibration and noise of PMSMs have been studied extensively, e.g., the multi-physics field calculation of the radial electromagnetic force on the vibration and noise of permanent magnet motors is used [5]. In [6] to [8], the vibration and noise have been improved by suppressing torque ripple through magnet offset, stator-rotor core surface slotting and magnetic flux barrier optimization, respectively. There are many other effective measures to reduce the torque ripple and noise [9], [10], [11]. For segmented rotor skewed PMSM, [12] and [13] compared the vibration and noise characteristics of PMSMs with different skewed rotor designs, where [12] investigated the correlation between the breathing vibration shape and radial electromagnetic forces of the critical slot order. Theoretical analysis and finite element simulation show that the effect on the vibration and noise of different skewed design is greatly different because there are

The associate editor coordinating the review of this manuscript and approving it for publication was Alfeu J. Sguarezi Filho.

several axial modes. In [13], the torsional vibration and noise resonance are well correlated with the torsional modes of the motor stator in absence of detailed tangential forces illustration. As the countermeasures, one symmetrical V-shaped rotor skew and one staggered Z-shaped rotor skew are compared with the original step-skewed rotor design. Both papers have explored the distribution of the axial electromagnetic force due to the segmented skewed rotor.

The background of this study is that an unintended noise spike occurs in the sensitive low-speed range when integrating a PMSM, which minimizes torque ripple by means of a step-skewed rotor into a coaxial eAxle. The objective of the study is to figure out the root cause of this noise spike, especially the relationship between electromagnetic force excitation and system structure response, and ultimately to find an effective method to identify such types of noise risks and optimize the motor design. Following this sequence, Section II starts with the modal analysis and then applies the operational deflection shape (ODS) method to verify the vibration profile. On the other side, in Section III, the contribution of radial and tangential forces to the noise is analyzed using the structural finite elements method. Based on the analysis and test results, a phase-based tangential force array analysis method is proposed in Section IV. It focuses on the dynamic time-variation process of the force related to each rotor segment. As the method reveals the coupling between the force array and the vibration, two symmetrical V-shaped skewed rotors with different adjacent angles are investigated and compared by means of this method. Furthermore, their comparison analysis results are validated by acoustic tests in an anechoic room and details are described in Section V. Section VI summarizes and concludes the whole article.

II. THE NOISE SPIKE OF A COAXIAL EAXLE

A. TORQUE RIPPLE OPTIMAL SEGMENTED SKEW PMSM

Electric axle integrates electromechanical devices such as drive motor, gearbox, and differential and are widely used in electric vehicles. According to the layout of the motor shaft and the gearbox output shaft, eAxle can be divided into two categories: parallel shaft eAxle and coaxial shaft eAxle [14]. The output shaft of the coaxial gearbox is connected to the half-shaft through the hollow motor shaft, which does not take up additional vehicle space and is more compact. For integer-slot PMSMs, step-skewed rotor segments are usually taken to weaken the tooth harmonics, which have a negative impact on the torque ripple. In this paper, the acoustic performance of an 8-pole 48-slot PMSM whose torque ripple is reduced to minimal by means of adjusting the shift angle between neighboring rotor segments is investigated. The torque ripple reaches a minimum value when the angle increases to 1.6°. The average torque value is 312.6Nm, and the torque ripple (ratio of ripple to average value) is 1.2%. Table 1 shows the main electromagnetic design parameters. Four permanent magnets (PMs) are configured with a double-V shape per pole. Fig. 1 shows the peak torque characteristics under rated voltage. The maximum vehicle speed is 230 kph, which corresponds to the motor shaft speed of 16000 rpm. Considering the background noise, the noise performance at low and medium speed ranges is especially important.

TABLE 1. Main electromagnetic design parameters.

Parameter	Value	Parameter	Value
Poles	8	Peak power	117 kW
Slots	48	Peak torque	310 Nm
Stator diameter	220 mm	Peak current	490 A
Stack length	135 mm	Rated voltage	320 Vdc
Rotor skew way	Step-skew	Knee point speed	3600 rpm
Segments no.	6	Maximum speed	16000 rpm
PM configuration	Double-V	Winding type	Hairpin

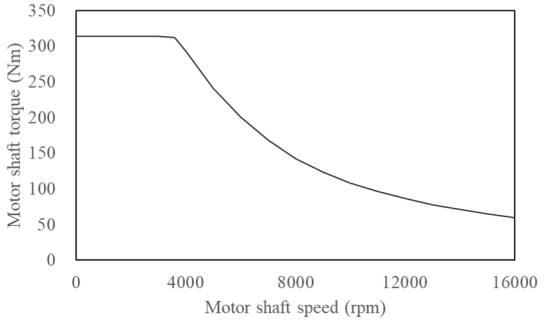

FIGURE 1. Peak torque characteristics under rated voltage.

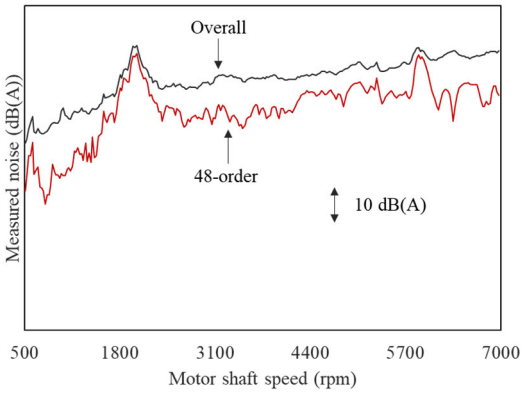

FIGURE 2. Measured noise of the optimal solution for torque ripple.

The eAxle was tested in an anechoic room and ran along the peak torque curve from a standstill to 7000 rpm. Five sound pressure sensors were placed one meter away from the eAxle surface and monitored the noise from 50 rpm. All of them captured the noise spike at about 2000 rpm. Fig. 2 shows the detailed results at the top position. The black line is the overall noise containing motor and gear orders, and the red line is the 48-order noise. As can see from this figure, the spike is nearly all contributed by the 48-order noise.

To figure out the root cause of the noise spike, it is necessary to analyze the correlation between the 48-order electromagnetic force and the system mode behind the spike.

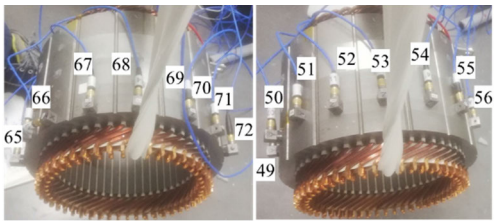

FIGURE 3. Modal testing of stator cores and windings.

B. MODAL ANALYSIS OF THE COAXIAL EAXLE

The eAxle is generally mounted to the subframe via several suspension points, and the system mode is close to the free state. The housing structure and mounting method are of great differences from traditional single-motor systems. Detailed mode analysis of the eAxle system is taken as following two steps: (1) motor stator system, (2) eAxle system.

1) MODAL ANALYSIS OF MOTOR STATOR SYSTEM

As the stator core is the entity on which the electromagnetic force acts directly, the accuracy of its mechanic parameters on modes is very important for the analysis accuracy of eAxle system modes. On the other side, the surface of the stator core is much smoother than the system housing. It can be facilitated the arrangement of more sensors to get higher accurate modal test results. The modal test was performed by means of the multiple-tapping method. It was completed in 10 times. Each time 8 three-way accelerometers were arranged along the circumference, then move to the next circle along the axial direction to repeat the test. Finally, there are a total of 240 signals for 80 positions. Fig. 3 shows the stator system containing the stator yoke, stator teeth, and a set of rectangular hairpin wire windings. The numbers near the sensors indicate the positions of 49 through 72 of a total of 80 positions.

To compare test and simulation results, the axial profile of the stator core is defined as XY plane, the axial direction as Z direction, XZ as the longitudinal section, YZ as the transverse section. The steel lamination sheet is isotropic in the XY plane and anisotropic in the XZ and YZ planes. The mass of the hairpin windings is equivalently counted into the stator teeth, with an overall density of 12.4 kg/dm^3. The equivalent Young's modulus $E_X = E_Y = 290$ GPa, $E_Z = 180$ GPa. The shear modulus $G_{XY} = 70$ GPa, $G_{XZ} = G_{YZ} = 11.6$ GPa. The Poisson's ratio is set at 0.29.

The modal test and simulation results are shown in Table 2, where *m* indicates the axial order and *n* indicates the radial order.

2) MODAL ANALYSIS OF COAXIAL EAXLE SYSTEM

Fig. 4 shows a cross-sectional view of the eAxle, which is mounted to the subframe via four suspension points: left front (LF), left rear (LR), right front (RF) and right rear (RR). The gearbox is directly connected to the motor. Their cast aluminum housing is combined and treated as an isotropic material with a density of 2.7 kg/dm^3, a Poisson's ratio of 0.34 and a Young's modulus of 75 GPa.

For the rotating parts of the eAxle, their mass is taken to be distributed to the supporting surfaces of the housing, i.e., the mass of the motor's rotating shaft is distributed to the bearing seats on the drive side and the non-drive side, and the mass of the gearbox's rotating parts is distributed to the bearing seats on the input side and the output side of the gearbox.

Based on the parameters from the stator system modal test, the coaxial eAxle system modes are analyzed. Fig. 5 shows the mode of 1755 Hz, where two diagrams represent two different moments. The arrow indicates the direction, and the length represents relative size of angular displacement at the moment. The torsional amplitude on the motor cover side is relatively small, and the amplitude on the gearbox side is relatively large. The greatest torsional displacement occurs around the RR position.

TABLE 2. Stator system modal simulation and testing.

Mode (m, n)	Measured (Hz)	Simulated (Hz)	Error (%)
(0,2)	688.2	688.7	0.01
(0,3)	1824.5	1812.4	0.66
(1,2)	1061.4	1138.9	7.3
(1,3)	1878.3	2031.2	8.14

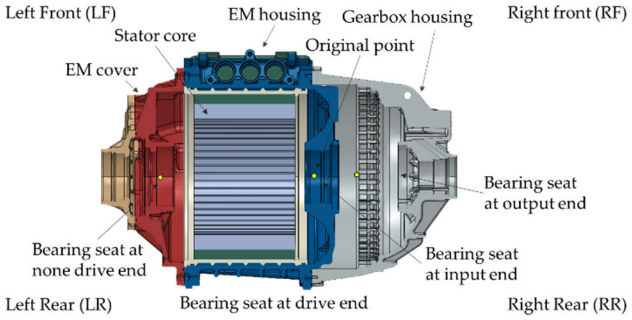

FIGURE 4. Longitudinal cross section view of the coaxial electric axle.

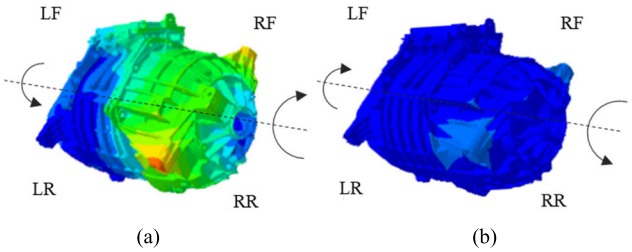

FIGURE 5. Torsional mode of the coaxial electric axle: (a) Moment 1; (b) Moment 2.

C. OPERATIONAL DEFLECTION SHAPE VALIDATION

As an effective method to identify the deflection of the specified noise spike [15], [16], the ODS test is performed to compare the deflection shape and the modal shape shown in Fig. 6. To obtain the correct result, it needs enough signals

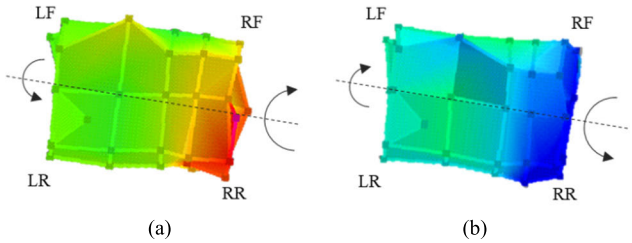

FIGURE 6. ODS measured profile variation at 2000rpm: (a) Moment 1; (b) Moment 2.

to describe the deflection profile. A similar approach to the modal test was used. Five tests are performed with eight sensors distributed in different axial positions each time. In addition, there are four sensors on four suspension points. Therefore, a total of 132 signals is applied to describe the profile variation. The mesh grid in the modal simulation is mapped to restore the deflection of the system housing surface. As shown in Fig. 6(a) and Fig. 6(b), the coaxial eAxle system profile is represented at two moments, with the arrows and lengths indicating the direction and magnitude of the torsion at the current moment, with the left side having a smaller torsion and the right side a larger one, particularly near the right rear mounts. The animation shows the profile variation is very close to the torsional mode variation shown in Fig. 5.

The measured noise spike occurs at about 2000 rpm, corresponding to a 48-order vibration noise frequency of 1600 Hz. The simulated torsional mode of the coaxial eAxle system is at 1755 Hz. There is an error of 9.7%, mainly due to two reasons: firstly, the simulation simplifies the mass distribution of the rotational systems of gearbox and motor, and secondly, as shown in Table 1, the simulated axial first-order modal error of the stator system is larger than the zero order.

III. ANALYSIS OF TANGENTIAL ELECTROMAGNETIC FORCE ARRAY

The ODS verified that the main modal contribution to the 2000 rpm noise spike is the first-order torsional mode of the system. To understand how electromagnetic forces excite the torsional modes, an analysis of the array of electromagnetic forces is proposed.

A. RADIAL AND TANGENTIAL FORCE CONTRIBUTIONS

Based on previous analysis, it is reasonable to assume that the torsional vibration is mainly excited by tangential electromagnetic forces. To verify this assumption, a series of analyses on the electromagnetic field and acoustic field are carried out in the following steps:

1) The electromagnetic forces on the stator nodes are obtained from the electromagnetic field finite element analysis, which is shown in Fig. 7(a). Most forces are acted on the stator surface of the inner diameter.
2) Decompose each nodal force into the radial and tangential components, which are shown in Fig. 7(b) and Fig. 7(c). They show that nearly all radial forces and most tangential forces are distributed on the stator surface of the inner diameter, while a few tangential forces act on both sides of each tooth near the slot open. And due to the complex composition of the spatial order, the force distribution on each tooth surface is uneven.
3) All three kinds of forces in Fig. 7 are mapped into a three-dimensional structural finite element model, with the mapping process considering the phase shift between skewed rotor segments.
4) Based on the simulated system modal results, vibration response of the system could be obtained using the modal superposition method.
5) The housing surface vibration is mapped onto the inner surface of the acoustic mesh. The A-weighted sound pressure is calculated at the five positions using the software LMS Virtual.lab 13.7.

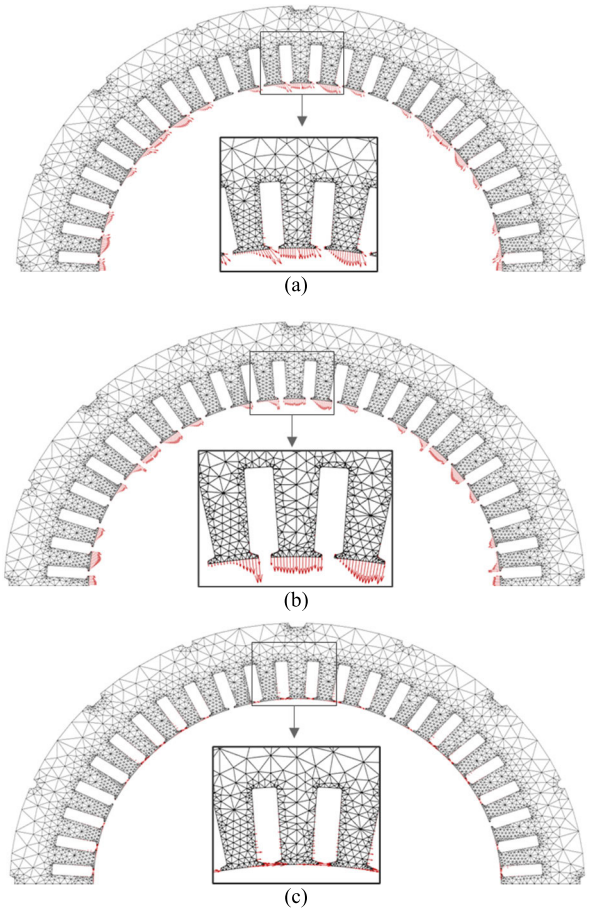

FIGURE 7. Nodal force distribution on the stator: (a) Electromagnetic force; (b) Radial force; (C) Tangential force.

Fig. 8 shows the simulation results from vibration to a sound field in the form of a system profile. To approach the realistic test scenario of the anechoic room, a flat ground surface is created to simulate the sound reflection. Also, an acoustic response surface surrounding the eAxle is created to cover the positions of five microphones. As radial and

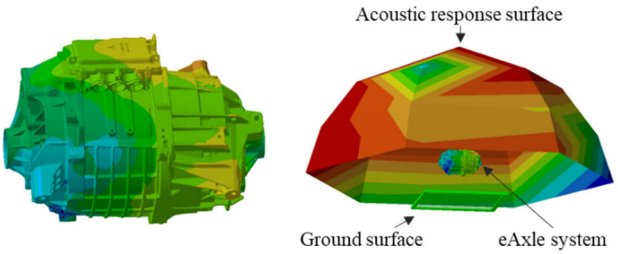

FIGURE 8. System profile of simulations from vibration to sound field: (a) Vibration simulation; (b) Sound field simulation.

TABLE 3. Sound field simulation results.

Implemented force	Only Tangential force	Only radial force	Both forces
Average noise dB(A)	75.3	39.6	75.6

tangential forces were applied on the stator surface respectively, 48-order cut level was calculated and summarized in Table.3. It shows that tangential force makes much more contribution to synthetic force than radial force, and torsional vibration is mainly excited by tangential electromagnetic forces.

B. THE 48-ORDER TANGENTIAL FORCE ARRAY

Based on the one-dimensional magnetic circuit, the magnetomotive force (MMF) of the stator and rotor are expressed as a Fourier series. And using the air gap permeability, the radial magnetic flux density expression can be obtained directly, and the radial force can be analyzed by substituting it into the force density equation. However, the tangential electromagnetic force is difficult to derive directly based on the one-dimensional magnetic circuit. It requires the solution of the two-dimensional electromagnetic field analysis. For PMSMs with complex rotor magnet arrangements, only numerical calculation methods can be well applied to account for the flux leakage. However, the tangential magnetic force density p_t still can be analytically expressed in terms of the line current density b and radial flux density a [1]:

$$p_t = b\,(x,t)\cdot a\,(x,t) \tag{1}$$

where t and x represent that both flux density and line current density alter with time-dependent and space-dependent. The ν-th space harmonic of the line current density interacts with the μ-th space harmonic of the rotor magnetic flux density to produce a tangential force density $p_{t\nu\mu}$ of

$$p_{t\nu\mu} = b_{2\mu}\,(x,t)\cdot a_{1\nu}\,(x,t) \tag{2}$$

where subscripts 1 and 2 indicate the stator and rotor, respectively. The μ-th harmonic of the radial magnetic density of the rotor $b_{2\mu}$ is

$$b_{2\mu} = B_{2\mu}\sin\left(\mu p\omega t - \mu\frac{\pi}{\tau}x - \varphi_{2\mu}\right) \tag{3}$$

TABLE 4. The amplitudes and phases of the 48th tangential mode corresponding to the six rotor skew segments.

Rotor Segment ID	Force amplitude (N/m^2)	Force phase (rad)
1	1724.3	-1.47
2	1971.2	-0.52
3	2067.6	0.47
4	2015	1.49
5	2142.7	2.55
6	2388.1	-2.64

where $B_{2\mu}$ is the rotor μ-th radial magnetic density amplitude, τ is the pole pitch, p is the number of pole pairs, ω is the mechanical angular frequency, and $\varphi_{2\mu}$ is the initial phase angle of the μ-th magnetic field in the airgap. The ν-th harmonic of stator line current density $\alpha_{1\nu}$ is

$$a_{1\nu} = A_{1\nu}\sin\left(p\omega t - \nu\frac{\pi}{\tau}x - \varphi_{1\nu}\right) \tag{4}$$

where $A_{1\nu}$ is the ν-th amplitude and $\varphi_{1\nu}$ is the initial phase angle of the ν-th component which is distributed along the circumference of the air gap. Substituting (3) and (4) into (2) yields the following equation.

$$\begin{aligned} p_{t\nu\mu}\,(x,t) = &-\frac{B_{2\mu}A_{1\nu}}{2} \\ &\times[\cos((\mu+1)p\omega t - (\mu+\nu)\frac{\pi}{\tau}x - \varphi_{1\nu} - \varphi_{1\mu}) \\ &+\cos((\mu+1)p\omega t - (\mu+\nu)\frac{\pi}{\tau}x - \varphi_{1\nu} - \varphi_{1\mu})] \end{aligned} \tag{5}$$

When $\mu = \pm\nu$, the force wave is uniformly distributed in the circumference direction, i.e., the spatial order is zero. Equation (5) can be simplified to

$$p_{t\nu\mu}\,(x,t) = -\frac{B_{2\mu}A_{1\nu}}{2}\cdot\cos\left((\mu\pm1)\,p\omega t - \varphi_{1\nu}\mp\varphi_{2\mu}\right) \tag{6}$$

When $\mu = 1$ or -1, the tangential force will not change with time. A constant torque is produced. When $\mu = 11$ or 13, the tangential force order is 48. For the zero spatial order of tangential force, there are the same values along the circumference at every moment. But they simultaneously change sinusoidally with time at 48 times the rotational frequency.

To elucidate the interrelationship of the 48^{-} order tangential electromagnetic force related to each rotor segment, a Fourier analysis of the tangential force density is performed to extract the amplitude and phase of the 48-order force of each segment. The results are shown in Table 4. The rotor segment numbers, 1-6, are corresponding to the positions in the eAxle from left to right.

It is difficult to see the characteristics of these six forces, especially if only their amplitudes are focused. As well known, the mechanism of Fourier analysis is to decompose complex waveforms into a series of simple sinusoidal waveforms. Therefore, it is proposed to graphically display the sinusoidal waveforms of these six tangential forces based on the amplitudes and phases in Table 4. As shown in Fig. 9, the

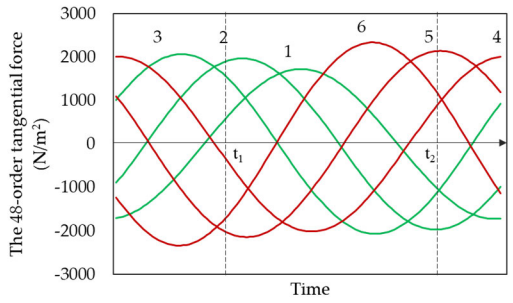

FIGURE 9. Simple sine waveforms of tangential forces of minimal torque ripple design.

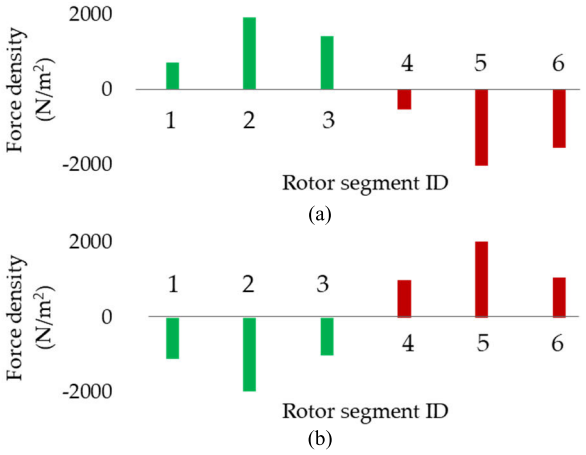

FIGURE 10. The 48th tangential force array: (a) t_1. (b) t_2.

green curves correspond to the three skewed segments on the left, and the red ones correspond to the three skewed segments on the right. The positive and negative amplitudes indicate forward and reverse rotational direction.

If we depict the changes in these six forces in the time domain, we can get an animation that represents them in an array. Each of them varies sinusoidally with time.

As shown in Fig. 10(a) and Fig. 10(b), the transient value of each force is observed at two moments, t_1 and t_2. A positive force at t_1 is generated corresponding to the left three segments; meanwhile, a negative force is produced corresponding to the right three segments. This phenomenon is reversed at t_2 as shown in Fig.10, in which the continuous change of each force vector over time is animated and arrayed together. The combined forces on the left and right sides can be observed to change in alternating positive and negative form. That is, these six electromagnetic forces exhibit a first-order torsional excitation. Thus, it makes a probability that the torsional 48-order tangential forces excite the torsional mode of the eAxle system as well as the noise spike. Because it is just due to the 48-order torsional excitation, the final noise spike is nearly only contributed by the 48-order component. It is different from the conventional structure resonance, which can be observed from various orders.

According to the electromagnetic force array analysis, for the PMSM with skewed rotor design, the torque ripple

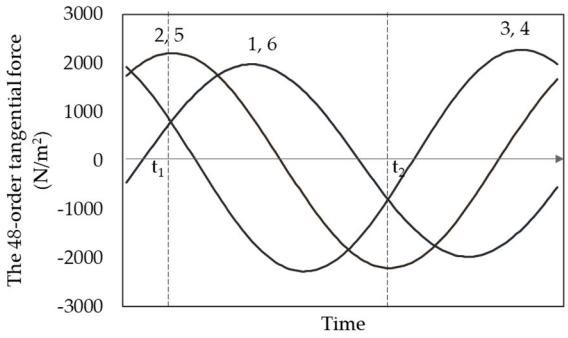

FIGURE 11. Simple sine waveforms of the 48th tangential forces of 1.8 symmetric V-shape skew design.

just reflects the total tangential forces related to all rotor segments. The detailed force array and their interaction are hidden.

IV. TANGENTIAL FORCE ARRAY OPTIMIZATION

After illustrating the mechanism between the excitation and response of the torsional spike, the optimization scheme can be considered in terms of an array of tangential electromagnetic forces. The straightforward approach is to replace the step-skewed rotor design with a symmetrical V-shaped rotor design because they have the same torsional direction at any time. However, it does not mean that all symmetrical V-shaped rotor designs are good for depressing the noise. The phase-based electromagnetic force analysis method is continued to compare their effects on vibration and noise.

Fig. 11 and Fig. 13 show the 48-order tangential force waves for two V-shaped rotor designs with different angles between adjacent rotor segments. The angle in Fig. 11 is 1.8° and that in Fig. 13 is 3.2°. Fig. 12 and Fig. 14 show their transient magnitude of the force for each rotor segment at the moments t1 and t2, respectively. It shows that although the left half and right half segments of the V-shape are symmetrical, there are still significant different force variations. The 48-order tangential forces of 1.8° show a simultaneous positive or negative direction most of the time. The 48-order tangential forces of 3.2° shows a more balanced array in positive and negative directions most of the time. Therefore, from the force wave behaviors, the V-shaped of 1.8° is like swing variation and not good for suppressing the torsional mode. For the 48-order tangential force of 3.2°, they can well depress the torsional mode because the vector sum of the forces respectively related to the left and right three segments are very small.

V. TEST AND VERIFICATION

Two symmetrical V-shaped PMSMs are integrated into the coaxial eAxles and acoustic tests are taken in an anechoic room to verify the effectiveness of the proposed method. Fig. 15 shows the full scene of the anechoic room and bench setup. Five microphones were placed at five positions to comprehensively capture the radiated noise. Each is one meter away from its nearest housing surface.

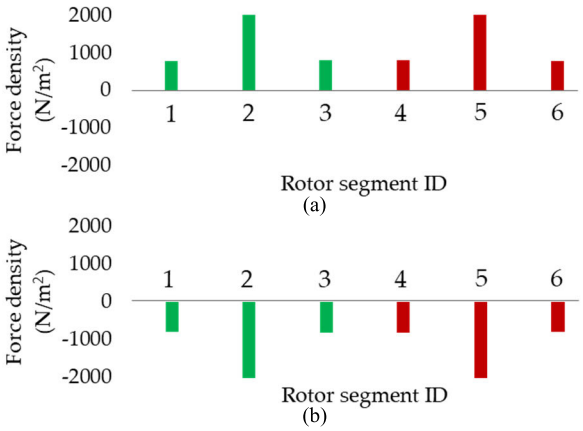

FIGURE 12. The 48th tangential force array: (a) t_1. (b) t_2.

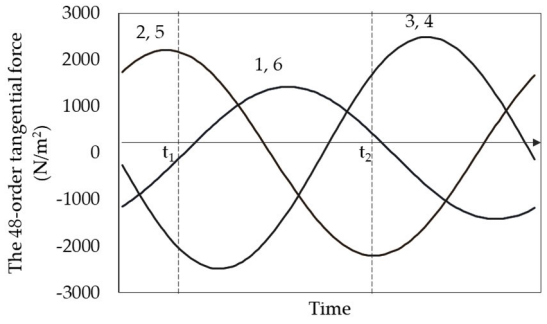

FIGURE 13. Simple sine waveforms of the 48th tangential forces of 3.2 symmetric V-shape skew design.

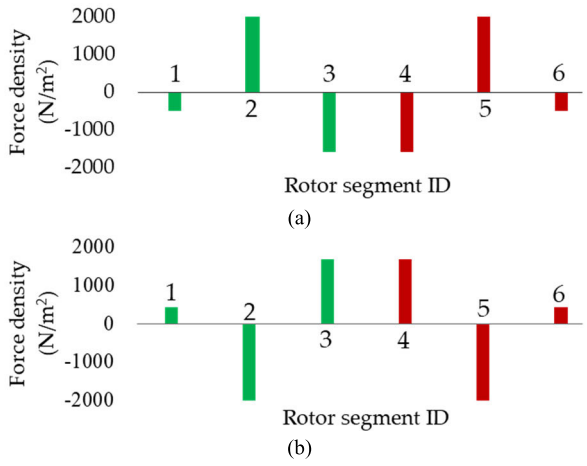

FIGURE 14. The 48th tangential force array: (a) t1. (b) t2.

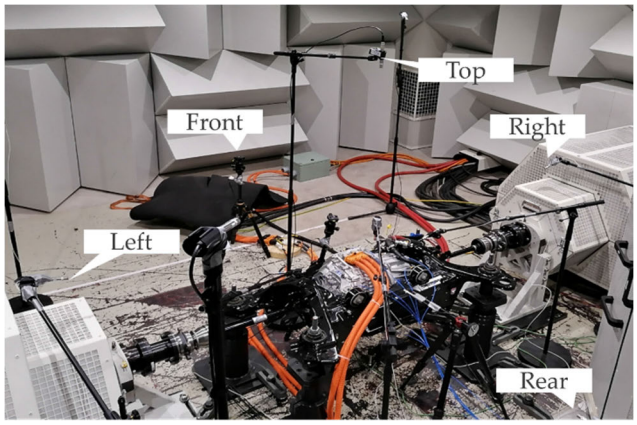

FIGURE 15. Tangential electromagnetic force arrays.

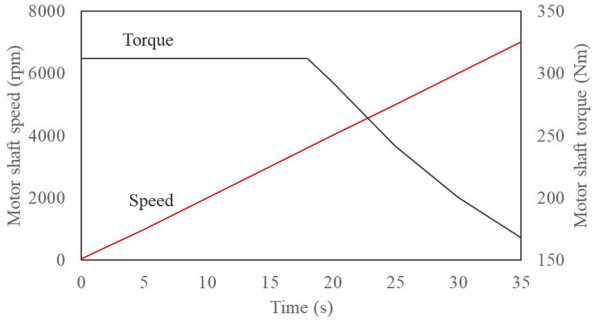

FIGURE 16. Simple sine waveforms of the 48th tangential forces of 1.8 symmetric V-shape skew design.

TABLE 5. Test sensor model and parameters.

Sensor	Model	Parameters
Microphone	PCB378B02	50 mV/g; 5-10 kHz frequency response
LMS FrontEnd	SCM205	

As shown in Fig. 16, they were run in torque mode along the outer characteristics. The speed is controlled by a bench dynamometer to complete the test exactly in 35 s so that sensor signals at each increment of speed can be tracked.

Table 5 lists the model and parameters of the sound sensor and processing equipment LMS FrontEnd [17] which is responsible for processing the signals with the sample frequency of 40 kHz. Fast Fourier Transform (FFT) method is used to analyze the data from the sensors. To reduce the leakage due to the non-periodic signals when applying FFT, a mathematical function called Hanning window [18] is employed to confine the leakage over a small frequency range instead of affecting the entire frequency bandwidth measured. After acquiring the spectrum of signals, the order analysis and order cut shall be started.

To accurately obtain the noise of specified order, it is crucial to specify the bandwidth. If the order bandwidth is set too narrow, some of the order energy will be excluded from the calculation. If the order bandwidth is set too wide, neighboring energy that is not due to the order energy will be included in the order cut. In this paper, the bandwidth is set to 0.5 order. That means all the energy between the 47.75-order and 48.25-order will be summed to the 48-order for each tracking rotational speed increment.

Fig. 17(a) and Fig. 17(b) show measured 48-order average noise of symmetrical V-shaped with 3.2° and 1.8° at five positions. The symmetrical V-shaped design with 1.8° and

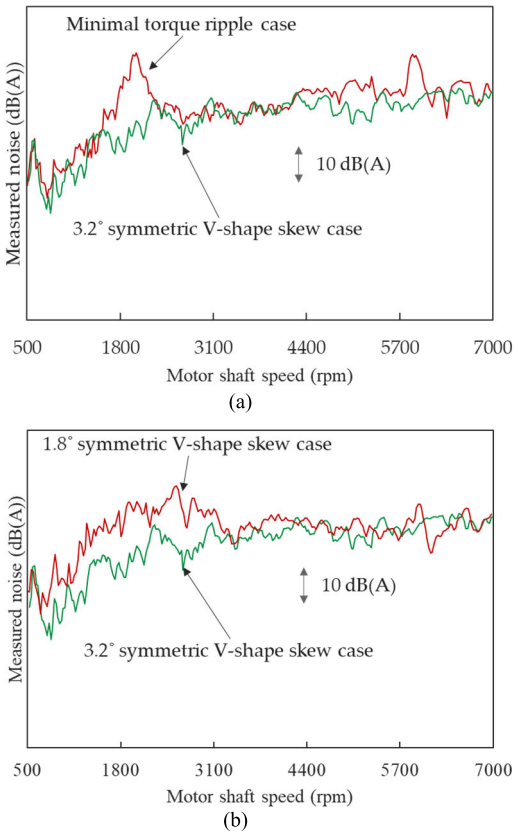

FIGURE 17. Comparison of measured noises: (a) Minimal torque ripple case and 3.2° symmetric V-shape skew case; (b) 1.8° symmetric V-shape skew case and 3.2° symmetric V-shape skew case.

the original step-skewed rotor design with 1.6° are compared to the symmetrical V-shaped design with 3.2°. As shown in the previous analysis, the symmetrical V-shaped design with 3.2° is much better than others over the concerned low-speed range. The torsional resonance is effectively suppressed around 2000 rpm. It is noted that the noises of the optimized symmetric V-shaped design did not become deteriorated at the knee point which corresponds the rated speed, 3600 rpm.

VI. CONCLUSION

In most situations, motor vibration and noise are mainly caused by radial forces. However, with the increasing of the peak torque density of the electric vehicle drive motor, the stator line current density, as well as the tangential components of the magnetic flux densities in the airgap, is much greater than that of the conventional motor. They not only result in an increase in tangential electromagnetic forces but also the tangential flux densities are no longer neglected when calculating the radial forces. In this paper, a graphical display of the sinusoidal variation for the 48-order tangential force array is proposed to analyze the noise spike of the coaxial eAxle system around 2000 rpm. The changing waveforms exhibited by the tangential force array are in good agreement with the vibration shape of the torsional mode. As the method interprets the coupling between the tangential force array and the torsional vibration, it provides a more targeted way for the shape optimization of the electromagnetic forces. Good noise performance is obtained after targeted improvement of the waveforms exhibited by the tangential force array. Specifically, the following conclusions can be drawn:

1) For the drive motor integrated into the electric coaxial axal system, the tangential forces play a very important role in the noise spike due to the system's torsional mode. As an important indicator for motor vibration and noise, torque ripple reflects the total tangential forces of all rotor segments whereas the torsional effect can use the proposed tangential force array to illustrate.

2) Not all symmetrical V-shaped rotor skew designs have a good noise performance. Only those with an appropriate adjacent angle can suppress the noise well. Those with inappropriate adjacent angle have a poor noise performance because the forces on the left half side and right half side exhibit simultaneous forward or reverse direction.

3) This paper focuses on the noise in low-speed range where the current lead angle is constant. The effect of suppressing the noise using rotor skew design is different in the high-speed range where the current lead angle and modes have altered. Nevertheless, the phase-based force array method provides a possibility that makes the variation of skew forces concisely and visually. It can also be applied to analyze the noise problems that are mainly caused by radial vibration modes, such as breathing mode.

REFERENCES

[1] J. F. Gieras, W. Chong, and L. J. Cho, "Preface," *Noise of Polyphase Electric Motors*. Boca Raton, FL, USA: CRC Press, 2006.
[2] Z. Q. Zhu and D. Howe, "Electromagnetic noise radiated by brushless permanent magnet DC drives," in *Proc. Electr. Mach. Drive Conf.*, 1993, pp. 606–611.
[3] Z. Q. Zhu and D. Howe, "Improved methods for prediction of electromagnetic noise radiated by electrical machines," *IEE Proc.-Electr. Power Appl.*, vol. 141, no. 2, pp. 109–120, Mar. 1994.
[4] N. Remus, M. S. Toulabi, S. Mukundan, H. Dhulipati, W. Li, C. Novak, and N. C. Kar, "Electromagnetic noise and vibration in PMSM and their sources: An overview," in *Proc. IEEE Can. Conf. Electr. Comput. Eng. (CCECE)*, Aug. 2020, pp. 1–4.
[5] D. Wang, W. Yang, J. Yang, K. Jiang, and Y. Fu, "Research on electromagnetic vibration characteristics of a permanent magnet synchronous motor based on multi-physical field coupling," *Energies*, vol. 16, no. 9, p. 3916, May 2023.
[6] X. Li, Z. Sun, W. Sun, L. Guo, and H. Wang, "Design of permanent magnet-assisted synchronous reluctance motor with low torque ripple," *World Electr. Vehicle J.*, vol. 14, no. 4, p. 82, Mar. 2023.
[7] J. Liang, Y. Dong, H. Sun, R. Liu, and G. Zhu, "Flux-barrier design and torque performance analysis of synchronous reluctance motor with low torque ripple," *Appl. Sci.*, vol. 12, no. 8, p. 3958, Apr. 2022.
[8] G. Liu, X. Du, W. Zhao, and Q. Chen, "Reduction of torque ripple in inset permanent magnet synchronous motor by magnets shifting," *IEEE Trans. Magn.*, vol. 53, no. 2, Feb. 2017, Art. no. 8100713.
[9] H. Ge, X. Qiu, B. Guo, J. Yang, C. Bai, and Z. Jin, "Optimized rotor shape for reducing torque ripple and electromagnetic noise," *IEEE Trans. Magn.*, vol. 58, no. 2, pp. 1–5, Feb. 2022.
[10] Y. Shimizu, S. Morimoto, M. Sanada, and Y. Inoue, "Investigation of rotor topologies for reducing torque ripple in double-layer IPMSMs for automotive applications," *IEEE Trans. Ind. Electron.*, vol. 70, no. 8, pp. 8276–8285, Aug. 2023.
[11] M. S. Islam, R. Mikail, M. A. Kabir, and I. Husain, "Torque ripple and radial force minimization of fractional-slot permanent magnet machines through stator harmonic elimination," *IEEE Trans. Transport. Electrific.*, vol. 8, no. 1, pp. 1072–1084, Mar. 2022.

[12] J. Blum, J. Merwerth, and H.-G. Herzog, "Investigation of the segment order in step-skewed synchronous machines on noise and vibration," in *Proc. 4th Int. Electr. Drives Prod. Conf. (EDPC)*, Sep. 2014, pp. 1–6.
[13] M. Arata, N. Takahashi, M. Mochizuki, T. Araki, and T. Hanai, "Torsional resonance noise reduction by motor torque phase adjustment," *World Electr. Vehicle J.*, vol. 5, no. 2, pp. 527–532, Jun. 2012.
[14] M. Mehrgou, I. G. de Madinabeitia, B. Graf, F. Zieher, and C. Priestner, "NVH aspects of electric drives-integration of electric machine, gearbox and inverter," SAE Tech. Paper 2018-01-1556, 2018.
[15] S. Khodaygan, "A method for system identification in the presence of unknown harmonic excitations based on operational modal analysis," SAE Tech. Paper 2019-01-5007, 2019.
[16] W. Peng, H. Tian, Y. Huang, M. Jin, Y. Zhang, and X. Wang, "Power transformer state identification method based on operational deflection shapes and visual measurement technology," in *Proc. IEEE 4th Int. Conf. Power, Intell. Comput. Syst. (ICPICS)*, Jul. 2022, pp. 51–54.
[17] (Jul. 23, 2023). *Simcenter Testlab*. [Online]. Available: https://community.sw.siemens.com/s/article/simcenter-testlab-signature
[18] A. V. Oppenheim, R. W. Schafer, and J. R. Buck. *Discrete-Time Signal Processing*. Upper Saddle River, NJ, USA: Prentice-Hall, 1999.

CHAO HUANG received the B.Eng. degree in mechanical engineering from Tongji University, Shanghai, China, and the M.Sc. degree from the Technical University of Munich, Munich, Germany. He is currently pursuing the Ph.D. degree in vehicle engineering with the School of Automotive Studies, Tongji University. His research interests include powertrain performance and dynamic control of new energy vehicles.

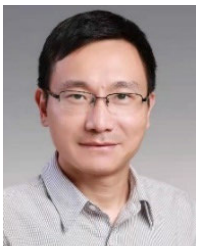

LU XIONG received the Ph.D. degree in vehicle engineering from Tongji University, Shanghai, China, in 2005. He is currently a Professor and the Deputy Dean of the School of Automotive Studies, Tongji University. He is also the Executive Director of the Institute of Intelligent Vehicles and the Associate Director of the Clean Energy Automotive Engineering Center, Tongji University. His research interests include perception, decision and planning, dynamics control and state estimation, and testing and evaluation of autonomous vehicles.

YU GONG received the B.Eng., M.Sc., and Ph.D. degrees from Shanghai University, Shanghai, China. He is currently a Staff System Engineer with Schaeffler, Shanghai. His research interest includes electrical machines with drive systems for new energy vehicles.

MINGYUAN JIANG received the B.Eng. degree in electrical engineering and automation from Shanghai Maritime University, Shanghai, China, in 2020, and the M.Sc. degree in electrical engineering from The Hong Kong Polytechnic University, Hong Kong, China, in 2021, where he is currently pursuing the Ph.D. degree in electrical engineering. His main research interests include design, optimization, and control of electric machine.

SHUANGXIA NIU (Senior Member, IEEE) received the B.Sc. and M.Sc. degrees from Tianjin University, Tianjin, China, and the Ph.D. degree from The University of Hong Kong, Hong Kong, SAR, China, all in electrical engineering. She is currently a Professor with the Department of Electrical and Electronic Engineering, The Hong Kong Polytechnic University. She authored or coauthored more than 100 articles in leading journals. She is currently an Associate Editor of the IEEE JOURNAL OF EMERGING AND SELECTED TOPICS IN POWER ELECTRONICS.